J|A|C|S
ARTICLES
Published on Web 07/14/2006

Electrochemistry, Spectroscopy, and Electrogenerated Chemiluminescence of Silole-Based Chromophores

Matthew M. Sartin, Andrew J. Boydston, Brian L. Pagenkopf, and Allen J. Bard*

Contribution from the Chemistry and Biochemistry Department, The University of Texas at Austin, Austin, Texas 78712

Received March 17, 2006; E-mail: ajbard@mail.utexas.edu

Abstract: We studied the electrochemical and spectroscopic properties of a series of extended silole-based chromophores to understand the effect of structure on behavior. By changing the substituents attached to the chromophore, we observed large variations in luminescence quantum efficiency (ca. 0−0.6), λ_{max} for absorbance and photoluminescence (PL), and radical ion stability. The differences are related to the motion in the 2,5-substituents and the steric protection of both the chromophore and the reactive parts of the substituents. For several compounds the electrogenerated chemiluminescence (ECL) spectrum was also compared to the photoluminescence spectrum. In all cases, the ECL λ_{max} and the PL λ_{max} were about the same.

Introduction

We report the electrochemistry and electrogenerated chemiluminescence (ECL) of a series of silole (1-silacyclopentadiene) compounds. There have been several studies of silole photoluminescence,[1−5] but chemiluminescence (CL) has been observed in only one instance.[6] There have also only been a few, brief studies of the electrochemistry of siloles, and few siloles are known to exhibit stable radical anions, while none showed stable radical cations.[1,2,7,8] Synthetically, siloles of broad structural diversity have been difficult to synthesize, and those most easily obtained from Tamao's cycloreduction protocol[9] generally show poor photoluminescence efficiencies.[10] It was recently observed, however, that judicious structural modifications could achieve high quantum yields from siloles derived via cycloreduction of bis(phenylethynyl)silanes.[11] These recent contributions have made possible the first series of homologous silole chromophores suitable for potential ECL studies. Given the unique molecular orbital properties of siloles, and their resultant applications in electron transport materials,[3,4,12−14] a better understanding of the relationship between the structural and electrochemical properties of these compounds is of interest, as is ECL in this class of compounds.

Siloles are interesting because of their low LUMO level compared with that of analogous conjugated cyclic compounds, such as furan, pyrrole, thiophene, and cyclopentadiene.[15] The suspected cause is a unique interaction between the π^* orbital of the butadiene moiety and the σ^* orbital of the exocyclic Si−R bond.[15] A narrow energy gap enables oxidation and reduction of a silole within the potential window of the solvent, which is necessary for ECL.[16]

In ECL, an anion and a cation are electrochemically generated and allowed to annihilate. The energy of annihilation is $-\Delta H^\circ = -\Delta G^\circ - T\Delta S^\circ$ ($T\Delta S^\circ \approx 0.1$ eV), where $\Delta G^\circ = E^\circ_{cation} - E^\circ_{anion}$. If ΔH° of annihilation is sufficient, one part of the annihilating pair will be left in an excited state. The simplest reaction scheme is as follows:

$$R + e \rightarrow R^{\bullet -} \quad (1)$$

$$R - e \rightarrow R^{\bullet +} \quad (2)$$

$$R^{\bullet -} + R^{\bullet +} \rightarrow {}^1R^* + R \quad (3)$$

$$R^{\bullet -} + R^{\bullet +} \rightarrow {}^3R^* + R \quad (4)$$

$${}^3R^* + {}^3R^* \rightarrow {}^1R^* + R \quad (5)$$

(1) Yamaguchi, S.; Tomonori, E.; Uchida, M.; Izumizawa, T.; Furukawa, K.; Tamao, K. *Chem. Eur. J.* **2000**, *6*, 1683.
(2) Zhan, X.; Risko, C.; Amy, F.; Chan, C.; Zhao, W.; Barlow, S.; Kahn, A.; Brédas, J.-L.; Marder, S. *J. Am. Chem. Soc.* **2005**, *127*, 9021.
(3) Yu, G.; Yin, S.; Liu, Y.; Chen, J.; Xu, X.; Sun, X.; Ma, D.; Zhan, X.; Peng, Q.; Shuai, Z.; Tang, B.; Zhu, D.; Fang, W.; Luo, Y. *J. Am. Chem. Soc.* **2005**, *127*, 6335.
(4) Lee, J.; Liu, Q.-D.; Motala, M.; Dane, J.; Gao, J.; Kang, Y.; Wang, S. *Chem. Mater.* **2004**, *16*, 1869.
(5) Chen, J.; Law, C.; Lam, J.; Dong, Y.; Lo, S.; Williams, I.; Zhu, D.; Tang, B. *Chem. Mater.* **2003**, *15*, 1535.
(6) Janzen, E.; Harrison, W.; Dubose, C. *J. Organomet. Chem.* **1972**, *40*, 281.
(7) Yamaguch, S.; Endo, T.; Uchida, M.; Izumizawa, T.; Furukawa, K.; Tamao, K. *Chem. Lett.* **2001**, 98.
(8) Dhiman, A.; Zhang, Z.-R.; West, R.; Becker, J. Y. *J. Electroanal. Chem.* **2004**, *569*, 15−22.
(9) Tamao, K.; Yamaguchi, S.; Shiro, M. *J. Am. Chem. Soc.* **1994**, *116*, 11715.
(10) (a) Yamaguchi, S.; Endo, T.; Uchida, M.; Izumizawa, T.; Furukawa, K.; Tamao, K. *Chem. Eur. J.* **2000**, *6*, 1683−1692. (b) Lee, J.; Liu, Q.-D.; Motala, M.; Dane, J.; Gao, J.; Kang, Y.; Wang, S. *Chem. Mater.* **2004**, *16*, 1869−1877. Increased quantum yields (21%) have been obtained from 3,4-diarylsiloles via aggregation-induced emission, see: (c) Luo, J.; Xie, Z.; Lam, J. W. Y.; Cheng, L.; Chen, H.; Chengfeng, Q.; Kwok, H. S.; Zhan, X.; Lui, Y.; Zhu, D.; Tang, B. Z. *Chem. Commun.* **2001**, 1740−1741. (d) Chen, J.; Xie, Z.; Lam, J. W. Y.; Law, C. C. W.; Tang, B. Z. *Macromolecules* **2003**, *36*, 1108−1117. (e) Chen, J.; Law, C. C. W.; Lam, J. W. Y.; Dong, Y.; Lo, S. M. F.; Williams, I. D.; Zhu, D.; Tang, B. Z. *Chem. Mater.* **2003**, *15*, 1535−1546.
(11) Boydston, A. J.; Pagenkopf, P. L. *Angew. Chem., Int. Ed.* **2004**, *43*, 6336.
(12) Tamao, K.; Uchida, M.; Izumizawa, T.; Furukawa, K.; Yamaguchi, S. *J. Am. Chem. Soc.* **1996**, *118*, 11974.
(13) Uchida, M.; Izumizawa, T.; Nakano, T.; Yamaguchi, S.; Tamao, K.; Furukawa, K. *Chem. Mater.* **2001**, *13*, 2680.
(14) Tang, B. Z.; Zhan, X.; Yu, G.; Lee, P. P. S.; Liu, Y.; Zhu, D. *J. Mater. Chem.* **2001**, *11*, 2974.
(15) Yamaguch, S.; Tamao, K. *J. Chem. Soc., Dalton Trans.* **1998**, 3693.
(16) For reviews of ECL, see: (a) Richter, M. M. *Chem. Rev.* **2004**, *104*, 3003. (b) *Electrogenerated Chemiluminescence*; Bard, A., Ed.; Marcel Dekker: New York, 2004.

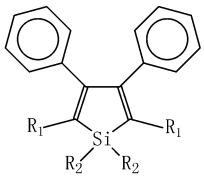

Compound	R_1	R_2
2a	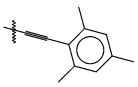	CH_3
2b	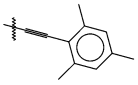	*t*-butyl
2c	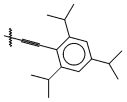	*t*-butyl
3a	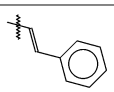	CH_3
3b	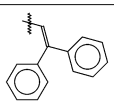	CH_3
3c	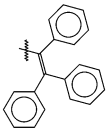	CH_3

Figure 1. Structure and names of each silole compound used.

Several criteria are important for annihilation ECL. Both the reduction and oxidation must occur within the potential window of the solvent. As mentioned earlier, the difference between the reduction and oxidation potentials must be greater than the energy of an excited state of one of the reactants. The radical anion and cation must be sufficiently stable to encounter one another before they are consumed by secondary reactions. Even small amounts of water or oxygen can often scavenge enough of the radical ions to prevent ECL, and some radical ions can dimerize or polymerize.[17,18] When generating ECL by pulsing an electrode between potentials for the oxidation and reduction of the substrate, it is often necessary to generate both the oxidized and reduced species in rapid succession so that they can react before scavenging processes become significant.

Recently, a series of highly luminescent (quantum efficiency, Φ_{PL}, as high as 0.60) 2,5-bis(arylethynyl)-substituted siloles were synthesized.[19] These, and a similar series of ethylene-substituted siloles (shown in Figure 1), form the basis of this study. Though they lack the structural rigidity that appears to minimize internal conversion in ethynyl-substituted siloles,[19] olefinic compounds are less susceptible to polymerization reactions upon reduction.[20] Eliminating such secondary reactions improves ECL stability. However, the ethynyl-substituted siloles were consistently more efficient fluorophores and generally exhibited greater radical ion stability than their ethylene-substituted counterparts. With increasing steric protection of the triple bonds, the ethynyl-substituted compounds exhibited increases in both fluorescence efficiency and radical ion stability, whereas the ethylene-substituted compounds exhibited decreasing quantum efficiency and radical stability with increasing steric protection. In this paper, we examine the structure of these compounds in an attempt to understand its impact on both their electrochemical and photophysical behavior.

Experimental Section

Materials. Anhydrous acetonitrile, benzene, and acetone were obtained from Aldrich (St. Louis, MO) and transferred directly into a helium atmosphere drybox (Vacuum Atmospheres Corp., Hawthorne, CA) without further purification. THF was distilled from sodium and benzophenone under a nitrogen atmosphere and degassed with argon prior to use with Li metal. $ZnCl_2$ was flame-dried under vacuum and stored in a drybox. Tetra-*n*-butylammonium perchlorate (TBAP) was obtained from Fluka and transferred directly into the drybox. All silole compounds except **3b** and **3c** were synthesized as previously described.[1,19]

Bis(diphenylethenyl) Silole (3b). A solution of bis(phenylethynyl)-dimethylsilane (**1**) (520 mg, 2.00 mmol) in THF (2.0 mL) was added dropwise into a THF solution of LiNaph (9.4 mL, 0.85 M, 8.00 mmol) under argon. The mixture was stirred for 10 min and then cooled in an ice−salt bath, and a solution of $ZnCl_2$ (1.36 g, 10.0 mmol) in THF (10 mL) was added rapidly via cannula. The ice−salt bath was removed and the mixture stirred for 30 min. In a separate dry flask equipped with a H_2O-jacketed condenser were added $Pd(PPh_3)_4$ (231 mg, 0.20 mmol), THF (5 mL), and 2-bromo-1,1-diphenylethene (1.14 g, 4.40 mmol) under argon. The silole solution was then added into the flask containing Pd via cannula under an argon atmosphere. The resulting mixture was heated at 50 °C and monitored by TLC. Upon completion (ca. 13 h), the mixture was allowed to cool, poured into a half-saturated NH_4Cl solution, and extracted with Et_2O (3 × 20 mL). The organic extracts were washed with brine (1 × 50 mL), dried ($MgSO_4$), filtered through silica gel (50% CH_2Cl_2/hexanes elution), and concentrated. Flash chromatography on silica gel (10% CH_2Cl_2/hexanes) provided 582 mg (94%) of the desired compound as a yellow powder: $R_f = 0.11$ (20% CH_2Cl_2/hexanes); ^{1}H NMR ($CDCl_3$, 400 MHz) δ 7.37−7.28 (m, 10 H), 7.16−7.01 (m, 20 H), 6.54 (s, 2 H), −0.85 (s, 6H); ^{13}C NMR ($CDCl_3$, 100 MHz) δ 158.5, 143.7, 143.4, 141.45, 141.37, 139.1, 132.0, 130.0, 129.9, 128.6, 127.9, 127.8, 127.6, 127.3, 126.9, 126.8, −4.2; HRMS *m*/*z* calcd for $C_{46}H_{38}Si$ [M^+] 618.2743, found 618.2743.

Bis(triphenylethenyl) Silole (3c). A solution of bis(phenylethynyl)-dimethylsilane (**1**) (1.302 g, 5.00 mmol) in THF (5.0 mL) was added dropwise into a THF solution of LiNaph (24 mL, 0.85 M, 25.0 mmol) under argon. The mixture was stirred for 10 min and then cooled in an ice−salt bath, and a solution of $ZnCl_2$ (3.41 g, 25.0 mmol) in THF (25 mL) was added rapidly via cannula. The ice−salt bath was removed and the mixture stirred for 30 min. In a separate dry flask equipped with a H_2O-jacketed condenser were added $Pd(PPh_3)_4$ (578 mg, 0.50 mmol), THF (12 mL), and 1-bromo-1,2,2-triphenylethene (3.69 g, 11.0 mmol) under argon. The silole solution was then added into the flask containing Pd via cannula under an argon atmosphere. The resulting mixture was heated at 40 °C and monitored by TLC. Upon completion (ca. 12 h), the mixture was allowed to cool, poured into hexanes (ca 150 mL), filtered through silica gel (30% CH_2Cl_2/hexanes elution), and concentrated. The crude material was recrystallized three times sequentially from hot ^{i}PrOH/hexanes to give 3.21 g (83%) of the desired compound as a yellow powder. Analysis of the ^{1}H NMR spectrum at variable temperatures suggested that the compound exists as a mixture of rotational isomers. Two crystallographically unique molecules were identified in the unit cell by X-ray analysis: ^{1}H NMR ($CDCl_3$, 400 MHz) δ 7.29−6.48 (m, 40 H), −0.23 (s, 6H), −0.27 (s, 6H), −0.34 (s, 6H); ^{13}C NMR ($CDCl_3$, 100 MHz) δ 155.6, 154.7, 144.9, 144.5, 144.3, 144.1, 144.0, 143.9, 143.7, 143.5, 143.4, 140.1, 139.5, 139.2, 139.1, 138.7, 138.6, 138.4, 131.6, 131.5, 131.0, 130.8, 130.7, 130.5, 128.7, 127.45,

(17) Dietz, R. In *Organic Electrochemistry*; Baizer, M., Ed.; Marcel Dekker: New York, 1973; pp 256−266.
(18) Eberson, L. In *Organic Electrochemistry*; Baizer, M., Ed.; Marcel Dekker: New York, 1973; pp 448−465.
(19) Boydston, A. J.; Pagenkopf, P. L. *Angew. Chem., Int. Ed.* **2004**, *43*, 6336.
(20) Chen, S.-A.; Shy, H.-J. *J. Polym. Sci.: Polym. Chem. Ed.* **1985**, *23*, 2441.

127.40, 127.2, 127.0, 126.6, 126.2, 126.0, 125.9, 125.5, 125.4, −1.2. −2.9. −5.1; HRMS *m*/*z* calcd for $C_{58}H_{46}Si$ [M^+] 770.3369, found 770.3376.

Scheme 1

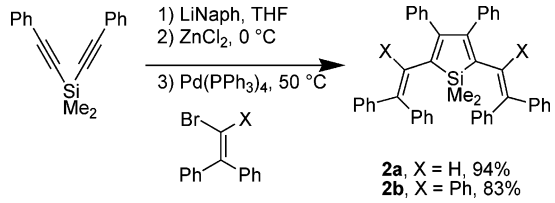

Characterization. Scheme 1 describes the synthesis of **3b** and **3c**. The procedure generates **3b** in 94% yield and **3c** in 83% yield. X-ray crystal structures (Figure S1) confirm the structures of these two compounds, and they show the orientation of the phenyl substituents with respect to the silole moiety in the solid state.

The electrochemical cell consisted of a coiled Pt wire as a counter electrode, a Ag wire as a quasi-reference electrode, and a 0.5 mm diameter Pt disk inlaid in glass. Fast-scan experiments (scan rate $\nu = 20-2000$ V/s) were performed with a 25 μm Pt disk inlaid in glass. At the end of an experiment, the Ag wire was calibrated with ferrocene (0.342 V vs SCE).[21] Before each experiment, the working electrode was polished on a felt pad with 0.3 μm alumina (Buehler, Ltd., Lake Bluff, IL) before being sonicated in deionized water and then ethanol for 1 min each. The electrode was then rinsed with acetone and transferred into the drybox. For ECL experiments, the working electrode was a ∼2 mm Pt disk bent at a 90° angle (J-type electrode), so that the disk faced the detector.

For electrochemical experiments, a 1 mM silole solution in 1:1 acetonitrile/benzene was prepared, and the solution was made 0.1 M in TBAP, the supporting electrolyte. All solutions were prepared inside the drybox. For measurements made outside of the box, the electrochemical cell was closed with a Teflon cap that had a rubber O-ring to form an airtight seal. Stainless steel rods driven through the cap formed the electrode connections. Cyclic voltammograms were obtained on a CH Instruments (Austin, TX) model 660 electrochemical workstation.

For photophysical characterization, various concentrations of silole were prepared in 1:1 benzene/acetonitrile in a 1 cm quartz cell. Electronic absorption spectra were collected on a DU 640 spectrophotometer (Beckman, Fullerton, CA). Fluorescence spectra were collected on a QuantaMaster spectrofluorimeter (Photon Technology International, Birmingham, NJ).

Digital simulations of cyclic voltammograms performed with the DigiElch software package[22] were used to investigate the mechanisms of the electrochemical processes. The uncompensated resistance and capacitance were determined by performing a potential step in the relevant solvent system in a region where faradaic reactions did not occur and using the potential step equations for the analogous RC circuit. Diffusion coefficients for each species were determined from potential steps to a diffusion-limited region and application of the Cottrell equation. For compounds that did not show simple, one-electron behavior, the diffusion coefficient (D) was approximated as 9×10^{-6} cm^2/s and adjusted to fit the data. Usually, no adjustment was necessary, as the value for all siloles was near 10^{-5} cm^2/s. The electrode surface area used in the simulations was determined by a potential step experiment performed in a solution of acetonitrile and ferrocene ($D = 1.2 \times 10^{-5}$ cm^2/s.)[23]

To generate ECL, the working electrode was pulsed between the oxidation and reduction potentials of the silole with a pulse width of 0.1 s. For the ECL spectra, the potentiostat was a Princeton Applied Research (Trenton, NJ) model 173 potentiostat/galvanostat used in conjunction with a Princeton Applied Research model 175 universal programmer, and the detector was a CH 260 charge-coupled device (CCD) camera from Photometrics (Tucson, AZ). The camera was cooled with liquid nitrogen between −100 and −120 °C. The spectra were calibrated with a Hg lamp after each measurement. ECL transients were obtained by excitation with an Eco Chemie (Utrecht, The Netherlands) Autolab potentiostat connected to a photomultiplier tube (PMT R4220p, Hamamatsu, Japan). The PMT was supplied with −750 V from a high-voltage power supply series 225 (Bertan High Voltage Corp., Hucksville, NY).

ECL quantum efficiencies were determined by comparing the peak currents of the largest ECL transients collected during potential pulsing to the transients of 9,10-diphenylanthracene pulse amperometry (DPA). These measurements are only accurate to about an order of magnitude.

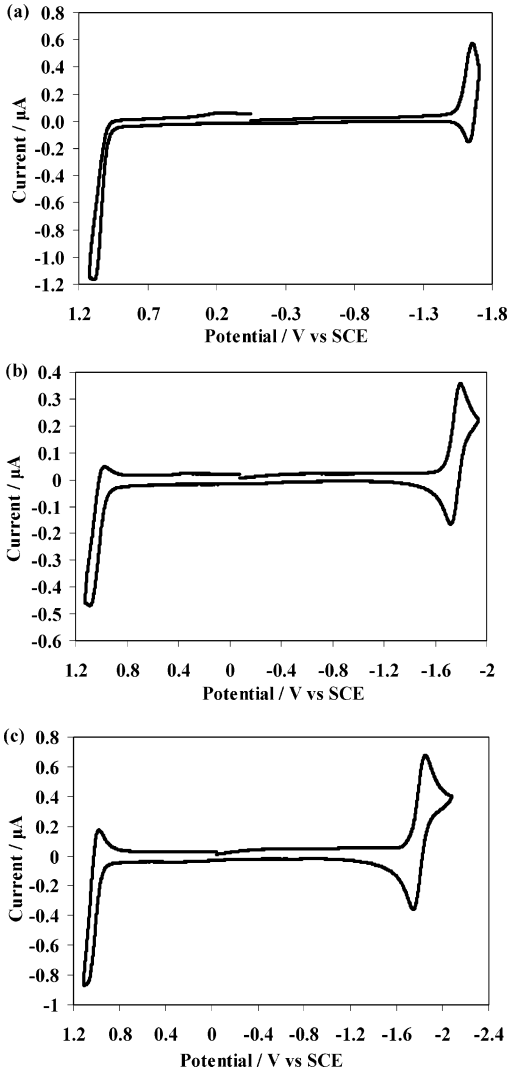

Figure 2. Cyclic voltammograms of 1 mM **2a** (a), **2b** (b), and **2c** (c) in 1:1 C_6H_6/MeCN with 0.1 M TBAP as the supporting electrolyte. Scans were made at 0.2 V/s.

Results and Discussion

Electrochemistry. (a) Ethynyl-Substituted Siloles. A summary of the electrochemical data for all siloles is given in Table 1, and cyclic voltammograms of the ethynyl-substituted siloles are shown in Figure 2. Reductions of **2c** and **2b**, at −1.80 and −1.76 V vs SCE, respectively, are one-electron, chemically

(21) Sahami, S.; Weaver, M. *J. Electroanal. Chem.* **1981**, *122*, 155.
(22) (a) Rudolf, M. *J. Electroanal. Chem.* **2003**, *543*, 23. (b) Ruldolf, M. *J. Electroanal. Chem.* **2004**, *571*, 289. (c) Rudolf, M. *J. Electroanal. Chem.* **2003**, *558*, 171. (d) Rudolf, M. *J. Comput. Chem.* **2005**, *26*, 619. (e) Rudolf, M. *J. Comput. Chem.* **2005**, *26*, 233. (f) Rudolf, M. *J. Comput. Chem.* **2005**, *26*, 1193.
(23) Kadish, K.; Ding, J.; Malinski, T. *Anal. Chem.* **1984**, *56*, 1741.

Table 1. Electrochemical Data for All Siloles[a]

silole	E_{red}, V vs SCE[b]	E_{ox}, V vs SCE[b]	ΔE	D, 10^{-6} cm^2/s	k°, cm/s[i]	reduction mechanism	oxidation mechanism
2a	−1.66[c] −1.68[d] −1.86[e]	0.99[g]	2.85	∼9	0.05[h]	complex; reversible above 1 V/s	irreversible two-electron
2b	−1.76	1.01	2.77	10	>d.c.[j]	reversible	ECE, $k_1 = 3$ s^{-1}
2c	−1.80	1.05	2.84	8.2	0.025	reversible	ECE, $k_1 = 1$ s^{-1}
3a	−1.76	0.83	2.59	18	>d.c.[j]	reversible	ECE, $k_1 = 4$ s^{-1}
3b	−1.82	0.86, 0.95[f]	2.70	12	0.05	reversible	EEC, $k_1 = 100$ s^{-1}
3c	−2.03[f]	0.93[g]	2.97	∼9	unknown[k]	unknown	irreversible two-electron

[a] All experiments were performed at a ∼0.5 mm Pt disk electrode in 1:1 benzene/MeCN with 0.1 M TBAP as the supporting electrolyte. [b] $E_{1/2} = (E_{p,c} + E_{p,a})/2$, except where otherwise specified. [c] Peak potential of prewave. [d] $E_{1/2}$ for the prewave at high scan rate, when it shows diffusional behavior. [e] $E_{1/2}$ for the diffusion wave that follows the prewave. ΔE_p for this wave is 140 mV. [f] Process is too complicated to measure $E_{1/2}$ in conventional ways, so it was estimated using the value required to make the simulated data fit. [g] Process is too fast to see reverse wave; peak potential was estimated as $E_{3/4}$ of the forward wave. [h] Determined at high scan rate, when adsorption peak behaved like a diffusional wave. [i] Heterogeneous rate constant for reduction reaction. [j] The heterogeneous electron transfer was faster than diffusion control (d.c.) at the highest scan rates employed (>1 cm/s).[24] [k] Irreversibility of the cyclic voltammogram prevents the use of ΔE_p to determine k°.

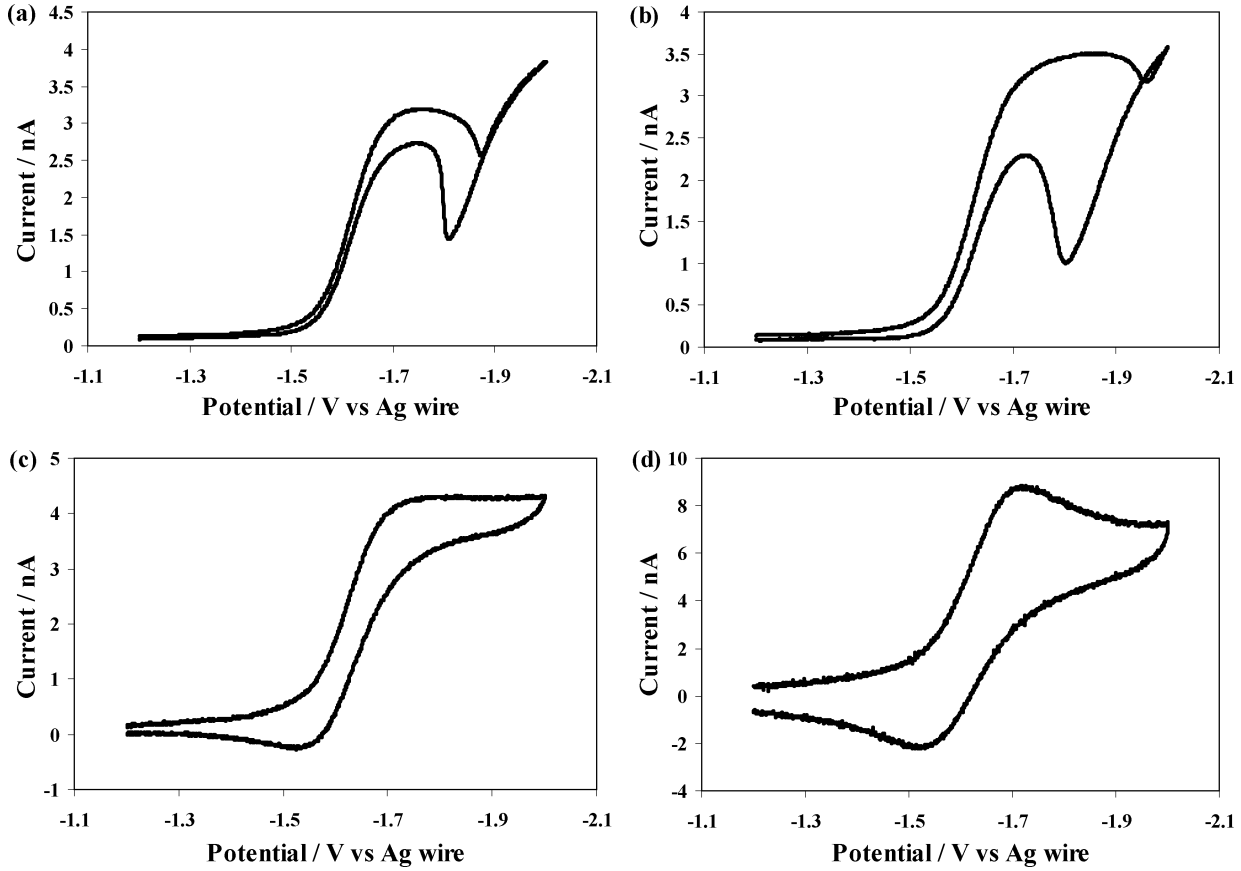

Figure 3. Cyclic voltammograms of **2c** performed at a 25 μm electrode scanned at (a) 0.01, (b) 0.05, (c) 0.5, and (d) 5 V/s. The sudden decrease in steady-state current at slow scan rates is attributed to an unstable blocking layer that forms during reduction.

reversible processes. However, the separation between the forward and reverse peaks (ΔE_p) for the reduction of **2c** is larger than the 59 mV expected for a nernstian reaction[24] (e.g., $\Delta E_p = 90$ mV at $\upsilon = 200$ mV/s). The uncompensated resistance, R_u, in this cell for the benzene/MeCN solution used was ca. 2 kΩ, which increases the apparent ΔE_p in the CVs. We also examined the CV of ferrocene (Fc), which shows a nernstian, one-electron oxidation at the scan rates used (50 mV/s to 10 V/s). Simulations of these CVs with this R_u value for Fc over the range of scan rates fit very well. However, even with R_u included in the simulations, the observed ΔE_p for the reduction of **2c** was significantly larger than that predicted for a nernstian reaction, suggesting that slow heterogeneous electron-transfer (HET) effects are significant with **2c**. Agreement between the experimental and simulated ΔE_p values for **2c** was only obtained with a heterogeneous reaction rate constant, k°, of 0.025 cm/s (Figure S2). This contrasts with the results for **2b**, where nernstian behavior was seen (i.e., k° is so large that HET does not compete with diffusional rates). Slow HET kinetics usually indicates a large reorganization energy for the molecule or the solvent. Organic compounds are often only weakly solvated and have very similar structures before and after the electron-transfer reaction; thus, they show fast HET.[25] However, **2c** is the most sterically crowded of this group of compounds, with isopropyl groups on the phenyl of the R_1 substituents, which could lead to significant reorganization of the molecule on electron transfer.

Attempts to simulate the CV of **2c** by adding homogeneous chemical reactions to the model, while leaving $k°$ large, were unsuccessful. For example, a C_rE mechanism, in which a first-order, reversible process precedes the electron transfer, as shown in eqs 6 and 7, could simulate intramolecular rotations of the

$$A \leftrightarrows B \quad (6)$$

$$B + e \rightarrow C \quad (7)$$

molecule that occur prior to electron transfer. This mechanism was simulated for various homogeneous rate constants for eq 6, with a fixed equilibrium constant. However, the predicted ΔE_p values for all rate constants studied in the simulations were less than the experimental data. For a small homogeneous rate constant, the voltammogram exhibited nernstian behavior, and for a sufficiently large rate constant, the forward peak appeared to flatten, while the ΔE_p remained unchanged. This shape change is not reflected in the experimental data, so it indicates an upper limit to practical simulations. The other possibility studied was the EC_r mechanism, in which a reversible homogeneous reaction follows the electrochemical step. In this case, simulations were made with the homogeneous rate constant held constant, while the equilibrium constant was varied. Again, the large ΔE_p was not observed. The voltammogram appeared nernstian when the equilibrium constant was small. When it was large, the voltammogram lost its reversibility, indicating an upper limit to practical equilibrium constants. Thus, we describe the large ΔE_p in terms of slow HET kinetics.

The reduction of **2a** at $v > 500$ mV/s results in a diffusion-controlled wave with a $k°$ of about 0.05 cm/s occurring at −1.68 V vs SCE. This wave shows chemically reversible behavior when the scan is reversed before −1.8 V (Figure S3). Upon scanning to more negative potentials, a second wave appears at about −1.86 V, and the anodic reversal wave of the earlier wave disappears. This effect appears to be associated with formation of some type of blocking film on the electrode, as can be seen from voltammograms taken at a 25 μm diameter Pt ultramicroelectrode (UME) (Figure 3). At low scan rates, where a typical steady-state voltammogram would show a diffusion-limited plateau, the steady-state current of **2a** drops when a blocking layer is formed but recovers partially on a reverse scan. Presumably, the film formation is a time-dependent process, and rapid scans can be made before filming becomes significant. Resolving the actual mechanism of this complex process will require further study.

The oxidations of **2a**, **2b**, and **2c** show irreversibility that is characteristic of radical cation instability (Figure 2). The anodic waves are also significantly larger (about double the corresponding initial reduction waves of the radical anions), suggesting further electron-transfer processes, i.e., ECE reaction sequences.[26] Simulations are consistent with **2b** and **2c** following ECEC mechanisms, with the first oxidations occurring about 1.01 and 1.05 V vs SCE, respectively (Figure S4). The potential for the second oxidation step for both of these compounds is

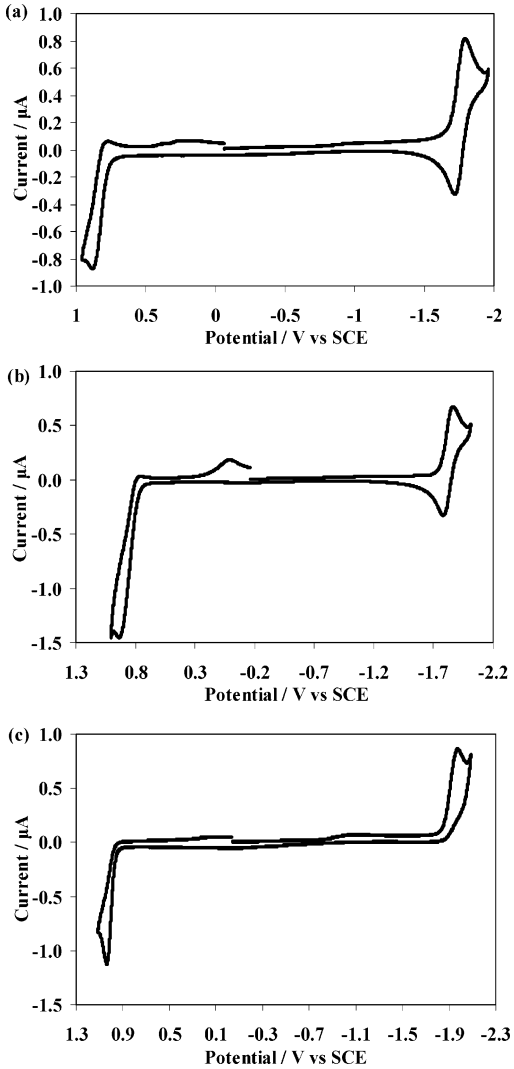

Figure 4. Cyclic voltammograms of 1 mM **3a** (a), **3b** (b), and **3c** (c) in 1:1 C_6H_6/MeCN with 0.1 M TBAP as the supporting electrolyte. Scans were made at 0.2 V/s.

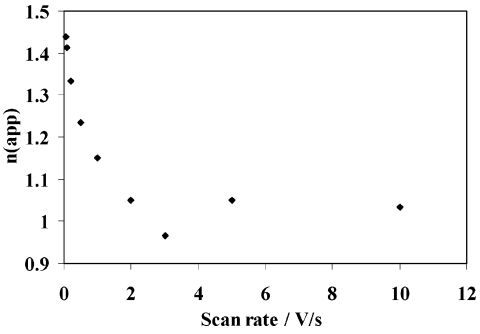

Figure 5. Plot of the apparent number of electrons versus scan rate for **3c**.

unknown, but in both cases, the second wave is indistinguishable from the first, which indicates that its potential is more negative than that of the first oxidation. Since this second wave is not involved in the ECL process, it was not investigated further. The following reactions for **2b** and **2c** were taken as first-order decompositions with rate constants, k_f, of 0.5 and 3 s^{-1}, respectively. In both cases, this homogeneous process could be the reaction of adventitious water with the radical cation. (Including higher order kinetics to account for this may improve the accuracy of the simulation but introduces more parameters

(24) Bard, A.; Faulkner, L. *Electrochemical Methods: Fundamentals and Applications*, 2nd ed.; John Wiley & Sons: New York, 2001; pp 234−238.
(25) Cauquis, G. In *Organic Electrochemistry*; Baizer, M., Ed.; Marcel Dekker: New York, 1973; pp 33−35.
(26) Bard, A.; Faulkner, L. *Electrochemical Methods: Fundamentals and Applications*, 2nd ed.; John Wiley & Sons: New York, 2001; pp 471−528.

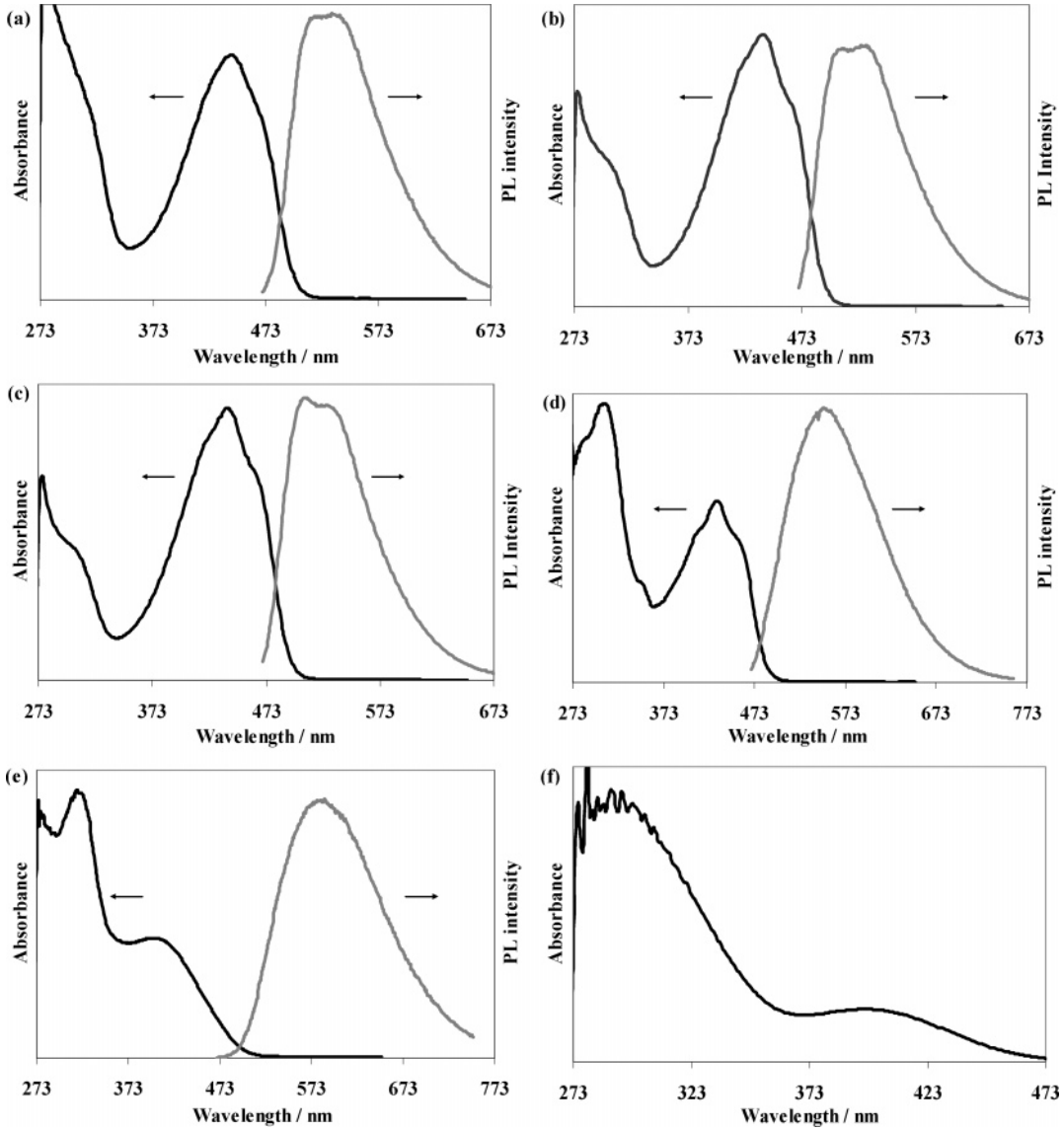

Figure 6. Absorbance and PL spectra (where applicable) of (a) **2a**, (b) **2b**, (c) **2c**, (d) **3a**, (e) **3b**, and (f) **3c** in 1:1 C_6H_6/MeCN. All compounds were excited at the absorbance peak wavelength.

than are useful to estimate.) The oxidation of **2a** was not simulated, as it showed no chemical reversibility for scan rates up to 2000 V/s, signaling a much faster decomposition of its radical cation. Comparison to the reduction wave peak height at 10 V/s suggests that the oxidation is a two-electron process.

The k_f values for decomposition of the radial cation follow the trend **2a** $\gg$ **2b** $>$ **2c**, suggesting that blocking of reactive sites, such as the triple bonds, is important. In **2b** and **2c**, the large 2,5-substituents and the *tert*-butyl groups on the silicon protect the triple bonds in the molecule from intermolecular reactions. The isopropyl groups on the phenyls are more protective than the methyls. The much higher reactivity of **2a** compared with that of **2b** suggests that the R_2 substituents on the Si are also important.

(b) Ethylene-Substituted Siloles. Compounds **3a**, **3b**, and **3c** reduce at about the same potentials as the ethynyl-substituted compounds. Interestingly, reduction of the ethylene-substituted siloles becomes more difficult as the number of phenyl groups attached to the ethylenes increases (Table 1 and Figure 4). This can be ascribed to a decrease in the conjugation of the phenyls with the remainder of the molecule because of steric interactions forcing the phenyls out of the molecular plane (Figure 2). To investigate further, quality crystals of **3b** and **3c** were obtained and analyzed by X-ray diffraction analysis (see Supporting Information). Indeed, the C2/C5 substituents of **3b** were rotated out-of-plane with the silole ring, thus reducing electronic communication along the chromophore backbone (average dihedral angle, 38°). Consistent with the electrochemistry and electronic absorption data (vide infra), the substituents on **3c** showed average dihedral angles of 55°, explaining the manifestation of even further reduced electronic communication (Figures S1 and S2).

Of the ethylene-substituted series, **3c** is the most difficult to reduce ($E_{1/2} \approx -2.03$ V vs SCE), probably because the interaction of the 2,5-phenyl groups on the triphenyethylene substituents forces the phenyls to rotate out of the plane of conjugation with the silole moiety. This illustrates the importance of the silole moiety in the conjugation of these compounds. Reduction of the **3a** is the easiest, occurring at -1.76 V vs SCE, as a reversible, one-electron process with fast heterogeneous kinetics. The reduction of **3b** is slightly more difficult (-1.82 V vs SCE), again because of disrupted conjugation. A k_s of

0.05 cm/s was required to match the simulated data to the experimental ΔE_p at high scan rates.

The reduction of **3c** is chemically irreversible at low scan rates (50 mV/s) but shows increasingly reversible behavior as the scan rate is increased (up to 10 V/s). The value of $i_{p,c}/\upsilon^{1/2}$, where $i_{p,c}$ is the cathodic peak current, decreases as the scan rate increases and becomes the one-electron value (based on the diffusion coefficients of the more well-behaved siloles) only for $\upsilon > 2$ V/s (Figure 5). This behavior suggests an ECE mechanism.[26] However, the absence of any anodic wave at low scan rates suggests that an irreversible homogeneous reaction also follows the second electron transfer, so the mechanism is actually ECEC:

$$A + e \rightarrow B \quad (8)$$

$$B \rightarrow C \quad (9)$$

$$C + e \rightarrow D \quad (10)$$

$$D \rightarrow F \quad (11)$$

We carried out simulations based on this mechanism assuming that both (9) and (11) are first-order reactions. The closest fit to the experimental data was obtained with $E_8^\circ = E_{10}^\circ = -2.03$ V vs SCE and $k^\circ = 0.015$ cm/s for both electron transfers, $k_9 = 3\ s^{-1}$ and $k_{11} = 0.5\ s^{-1}$. However, even this best fit showed considerable deviation from the experimental data (Figure S5), largely because at $\upsilon > 500$ mV/s there is additional cathodic current, perhaps caused by a small amount of adsorption of starting material or intermediates just beyond the reduction peak. Clearly, a fuller description of the reaction mechanism will require additional study in different solvents.

The oxidation waves of ethylene-substituted siloles at $\upsilon < 200$ mV/s are chemically irreversible, signaling a lower stability of the radical cations. In all cases, $i_{p,a}$ is larger than that of the initial reduction wave, indicating additional electron-transfer reactions. The oxidation of **3a** is an ECE reaction, with the first oxidation at 0.83 V vs SCE, and $k_f = 4\ s^{-1}$ for the following reaction. Again, the second oxidation occurs at a potential negative of the first oxidation (Figure S6). The oxidation of **3b** appears to be an EEC mechanism, with two distinguishable waves at $E_1 = 0.86$ V vs SCE and $E_2 = 0.95$ V, and $k_f = 100\ s^{-1}$ for the following reaction. The simulations (Figure S7) are only marginal, largely because of a third oxidation step that occurs slightly positive of the first two that adds to the forward anodic peak current. However, the general behavior of the waves fits an EEC mechanism better than the others, like ECE. The EEC nature of the oxidation of **3b** suggests that it can be considered as primarily involving removal of electrons from the 2,5-substituents rather than from a common orbital shared between the substituents and the silole ring, with only a weak interaction between the substituents. This makes sense if the two phenyls are rotated out of the plane of the molecule. The fact that $E_2 - E_1 = 90$ mV supports the idea of two weakly coupled oxidations (compared to an uncoupled system, where $E_2 - E_1 \approx 35$ mV).[27] Oxidation of **3c** is irreversible up to 2000 V/s. Comparison of the **3c** oxidation peak current to its reduction counterpart suggests that the oxidation of **3c** is a two-electron process, but we were unable to determine this quantitatively, due to the previously mentioned problems in the **3c** reduction.

(27) Bard, A.; Faulkner, L. *Electrochemical Methods: Fundamentals and Applications*, 2nd ed.; John Wiley & Sons: New York, 2001; p 507.

Table 2. Spectroscopic Data for Siloles: Absorbance and Fluorescence Measurements in Dichloromethane

silole	PL quant eff Φ[a]	abs max λ_{ABS}, nm	PL max λ_{PL}, nm	Stokes shift $\Delta\lambda$, nm	E_{PL}, eV	annihilation energy, eV	ECL eff[c]
2a	0.300	443	522	79	2.38	2.95	0.01
2b	0.630	439	529	90	2.35	2.87	0.1
2c	0.560	439	507	68	2.45	2.94	0.1
3a	0.183[b]	435	548	113	2.27	2.69	0.001
3b	0.016	433	584	151	2.13	2.8	0.01
3c	na	398	na	na	2.60	3.07	na

[a] Φ_{PL} determined with respect to fluorescein. [b] Tamao reports $\Phi = 0.047$ with respect to fluorescein.[1] [c] Represents the fraction of emission of a DPA cell under similar conditions. Accurate to about an order of magnitude.

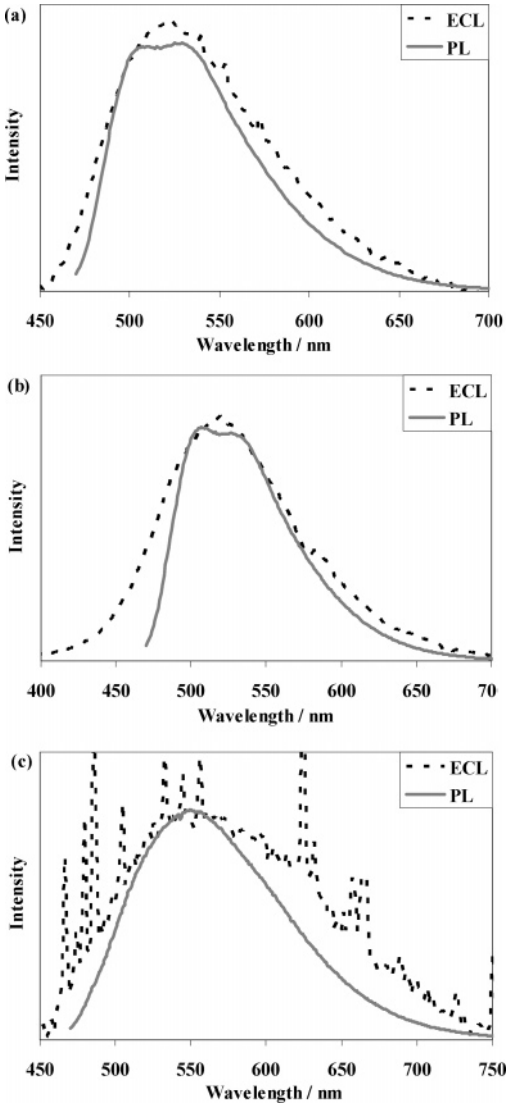

Figure 7. Overlays of ECL and PL spectra for (a) **2b**, (b) **2c**, and (c) **3a** in 1:1 C_6H_6/MeCN. No other compounds were sufficiently stable to obtain ECL spectra. Spectra were generated by pulsing between a potential approximately 100 mV past the peak potentials for reduction and oxidation of each compound. Pulse width for all compounds was 100 ms.

Spectroscopy. The absorbance and PL spectra are shown in Figure 6, and the results are summarized in Table 2. There are two peaks in the absorbance spectra. The shorter wavelength peak (partially perturbed by the absorbance of the solvent) is usually associated with the substituents,[14] and the longer wavelength peak is associated with the silole itself. The

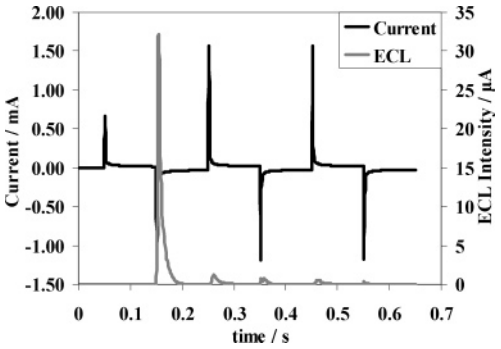

Figure 8. Intensity−time curve for **2a** ECL, generated by pulsing a single electrode at the first oxidation and first reduction potentials of the compound. The unstable radical cation of **2a** leads to a rapid loss of ECL intensity after multiple pulses.

absorption spectra of the silole with ethynyl substituents are slightly red-shifted from those of the silole with ethylene substituents. The λ_{max} for the three ethynyl-substituted siloles are very near one another, as expected, given the similarities in the structures. Of the spectra for siloles with ethylene substituents, that of **3c** is blue-shifted 33−35 nm with respect to those of **3a** and **3b**, consistent with the electrochemical data showing less conjugation of the crowded phenyl rings on the ethylene substituents in **3c** because of steric interactions.

All of the compounds, except **3c**, show fluorescence, with the ethynyl-substituted ones showing quite intense emission. Unlike the absorbance, the emission from **2c** is significantly blue-shifted from those of **2a** and **2b**. The smaller Stokes shift for **2c** could represent smaller reorganization in the excited state because of its steric rigidity. The ethylene-substituted compounds show larger Stokes shifts and smaller emission quantum efficiencies, probably because of the much greater flexibility of the substituents. The increasing number of phenyls in the ethylene-substituted series increases the number of degrees of freedom for internal conversion processes. This could explain the trend of decreasing quantum efficiency from **3a** to **3c**.

Electrogenerated Chemiluminescence (ECL). As can be predicted from the high photoluminescence quantum yield and reversible electrochemistry for reductive and oxidative processes, siloles **2c** and **2b** give well-defined ECL upon cycling between potentials on the first reduction and oxidation waves. These ECL spectra overlap their photoluminescence spectra, as shown in Figure 7. The PL spectra exhibit two peaks where the ECL spectra have only one, due to the wide slit width (∼1 mm) employed in the ECL measurements to capture the weaker emission. We were able to detect ECL with **2a** by pulsing the electrode with a 0.1 s pulse width and recording the total emission with a photomultiplier tube (Figure 8), but we were unable to obtain an ECL spectrum because its radical cation was too unstable. As shown in Figure 8, the initial ECL signal was intense, as would be expected from its high PL quantum efficiency, but it rapidly diminishes after a few pulses; similar behavior is observed for **3b**. While **3a** has a low fluorescence quantum yield, its homogeneous reactions are still slow enough that they do not compete with the time scale of the electrode pulses. Hence, this compound is also capable of stable ECL, and a spectrum was obtained for it as well (Figure 7c). In all cases where ECL was observed, the energy of the radical ion annihilation was sufficient to produce the energy of the singlet excited state.[16b]

Conclusions

The three ethynyl-substituted and three ethylene-substituted siloles show different trends in their electrochemical and photophysical behavior. The ethylene-substituted siloles have less steric rigidity, which gives them more ways to vibrationally dissipate energy; hence, they show lower fluorescence quantum efficiencies. To alleviate steric stress in **3b** and **3c**, the 2,5-substituents are forced to rotate out of the plane of the silole moiety, whereas **3a** can remain completely planar. Thus, the chromophores of **3b** and **3c** have less protection from secondary reactions upon oxidation or reduction. As a result, their radical ions are less stable, and they have lower fluorescence quantum yields than **3a** and poor ECL.

The ethynyl-substituted siloles are more sterically rigid. They show higher fluorescence quantum efficiencies than the ethylene-substituted siloles, but the unprotected triple bonds can lead to poor oxidative behavior. By adding *tert*-butyl groups to the silicon, the bonds are more protected from secondary homogeneous reactions. Thus, these compounds exhibit high fluorescence quantum efficiencies and produce ECL on radical ion annihilation.

Acknowledgment. We thank the National Science Foundation and BioVeris, Inc. for support of this research. A. J. Boydston also thanks The University of Texas at Austin for a Continuing Graduate Fellowship.

Supporting Information Available: X-ray crystallographic data for **3b** and **3c** (Figure S1 and CIF files) and additional CVs (Figures S2−S7). This material is available free of charge via the Internet at http://pubs.acs.org.

JA0618494